Journal of Applied Sciences and Nanotechnology

Journal homepage: jasn.uotechnology.edu.iq

Preparation and Characterization of Bi_2MO_6 (M = Mo, W) for Antibacterial Activity

[1]Huda N. Abid*, [2]Amar Al-Keisy, [1]Duha S. Ahmed, [3]Sangeeta Singh

[1]*Department of Applied Sciences, University of Technology – Iraq*
[2]*Nanotechnology and Advanced Materials Research Center, University of Technology – Iraq*
[3]*Microelectronics Lab, National Institute of Technology – India*

ARTICLE INFO

Article history:
Received: July, 17, 2022
Accepted: September, 13, 2022
Available online: June, 10, 2023

Keywords:
Bi-based photocatalysts,
Hydrothermal approach,
Nanosheets structure,
Growth inhibition zone

Corresponding Author:
Huda N. Abid
as.18.88@grad.uotechnology.edu.iq

ABSTRACT

Recently, bi-based photocatalysts have begun to be used in biological applications. However, the antibacterial ability of a Bi-based photocatalyst is still unclear. In this study, Bi_2MoO_6 and Bi_2WO_6 were successfully synthesised by a hydrothermal approach. The fabricated samples were characterised by X-ray diffraction, FESEM, and UV-Vis spectra. Besides, the antibacterial activity of both photocatalyst samples toward *E. coli* as unfavourable and S. aureus as positive pathogens were studied. Compared with the antibacterial of Bi_2WO_6, the resultant Bi_2MoO_6 exhibited high susceptibility to *S. aureus* bacterial strain, revealing large zones of 24 mm to 29 mm. Bi_2WO_6 exhibited less susceptibility of 17.5 mm to 21.5 mm compared with the zone of inhibition against tested bacterial *E. coli*. Besides, a possible mechanism suggested the effect of the nanosheet structure of samples to penetrate the cell membrane, which results in leakage of interior cell and complete death, and these results will provide some support for the applications of Bi_2MoO_6 and Bi_2WO_6 in antibacterial materials under typical environments.

https://doi.org/10.53293/jasn.2022.5250.1179, Department of Applied Sciences, University of Technology - Iraq.

1. Introduction

The deterioration of water quality caused by pathogenic has received public concern worldwide. Besides, antibiotic accumulation in water has seriously threatened environmental safety and human health [1]. As one of the most abundant bacteria in the environment, *E. coli* and *S. aureus* are always of great interest since they are pathogenic, harmless, and commonly found in food and water environments [1, 2]. Among the different fields, nanobiotechnology has represented a critical research area, with the increase in nanomaterials synthesis in several scientific studies as a possible alternatives for resistance to pathogens [3]. In recent years, green, efficient, and cost-effective Bi-based semiconductor photocatalysts have emerged as a more promising methodology than conventional technology of bacterial inactivation methods such as UV disinfection and chlorination [4–7]. Because of its high stability, strong redox potential, low cost, and non-toxic nature, TiO_2 has been extensively reported as an effective bactericidal semiconductor photocatalyst [8]. However, its band gap of 3.2 eV allows light absorption up to 387 nm, which accounts for just over 4% of the total solar spectrum. Because visible light (47 %) in solar radiation is more abundant than UV, efficient visible-light photocatalysts are required to use this proportion best [9]. Recently, Bi-based semiconductor technology has been considered a promising alternative to treat pathogenic microorganism pollution due to its clean and cost-efficient advantages without generating secondary pollution [3, 10]. Among these Bi-based photocatalysts, bismuth molybdates, Bi_2MO_6 (M=W, Mo) with the layered bismuth oxide family is of particular interest as a typical Aurivillius oxide due to its dielectric, ion-conductive, luminous, and catalytic properties [11–13]. A typical n-type semiconductor comprised of accumulating layers of alternating $(Bi_2O_2)^{2+}$ layers and $(MO_4)^{2-}$ octahedral sheets is also a promising visible-light-driven photocatalyst with good chemical and thermal stability, aside from its non-toxic and ecologically friendly nature [14, 15]. Moreover, Bi_2MoO_6 can degrade organic contaminants and exhibit high antibacterial effects under visible light irradiation [16, 17]. Besides, Bismuth tungsten Bi_2WO_6, representing the Bi-based photocatalysts, can produce strong oxidising free radicals that inactivate microorganisms and are very suitable for antibacterial treatment. Bi_2WO_6 has received much attention as active in visible light regions and is more advantageous for environmental treatment [18]. Despite the catalyst's lengthy history as a potential solution, most research on Bi_2MoO_6 has concentrated on the photocatalytic breakdown of organic pollutants, with only a few studies looking into the photocatalytic inactivation of microorganisms. A pseudo-first-order process observed *E.coli* degradation on Bi_2MoO_6 nest-like structures in a few hours [19]. Bi_2MoO_6 and Bi_2WO_6 have outstanding visible light photocatalytic activity due to their superior geometrical structural features [14, 20]. Constructing a unique micro/nano hierarchical structure typically shortens the paths of water contaminants, absorbs incidental light more efficiently due to increased multiple scattering, and is easily separated from wastewater by filtering or sedimentation processes [15, 21]. This paper synthesised Bi-based semiconductors like Bi_2MO_6 (M=W, Mo) using hydrothermal methods. The antibacterial effects and the proposed mechanism of the resulting nanosheets against the standard and multidrug-resistant *E.coli* as gram-negative and *S.aureus* as gram-positive bacteria were investigated.

2. Experimental Part

2.1 Synthesis of Bi_2MoO_6 and Bi_2WO_6 Nanoparticles

Based on prior research [22], a two-step hydrothermal technique was used to manufacture nanoplate Bi_2MoO_6 and Bi_2WO_6. $Bi(NO_3)_3$ (2 mmol) was first dissolved in 10 mL of nitric acid solution (HNO_3), then a 10-mL aliquot of Na_2MoO_4 solution (1 mmol) was dissolved and dropped into the $Bi(NO_3)_3$ solution while stirring. The blended solution's pH level was set at 4. The finished suspension was quickly transferred to a Teflon-lined 50-mL autoclave and cooked at 180°C for 15 hours in the second stage. Following that, the suspension was allowed to cool naturally at ambient temperature, and the solid result was cleaned multiple times before being dried in the air at 60^{o}C for 24h. Bi_2WO_6 nanoparticles were made using identical processes and amounts as Bi_2MoO_6 nanoparticles, but instead of Na_2MoO_4, Na_2WO_4 was used.

2.2 Characterisation

The XRD analysis of prepared samples was performed by Shimadzu X-ray diffraction 6000 diffractometer with CuKα radiation (λ=1.542 Å). Data were recorded in the 2θ range of 10^o-70^o. The band gap of the samples and the optical properties were recorded on a Shimadzu UV-1800 spectrophotometer. The surface morphology of samples was characterised by field emission scanning electron microscopy (FESEM, Mira3-XMU). Energy dispersive x-ray spectroscopy (EDS connected to FESEM) determined the chemical composition of produced samples.

2.3 Antibacterial Activity

The antibacterial activity of the resulting semiconductor, like Bi_2MO_6 (M=W, Mo), was evaluated against *E.coli* as unfavourable and *S.aureus* as positive pathogens by agar well diffusion assay [23, 24]. 25 µl of *E.coli* and *S.aureus* cultures suspension were prepared with initial concentration 106 (CFU\mL, McFarland tube No.0.5), incubated for 18h, and spread on the Mueller Hinton agar surface poured in Petri plates. Holes of 6 mm were made, and each hole was packed with different test concentrations of samples ranging from 50,100 and 200 µg\mL for each sample and using distal water (DW) as a negative control. The plates were wrapped with parafilm tape and incubated at 37^{o}C overnight. Negative controls using only *E.coli* and *S.aureus* were used. The bacterial growth inhibition zones were then measured in millimetres [25, 26].

3. Results and Discussion

3.1 Structural Properties

Fig. 1(a,b) shows the X-ray diffraction pattern of Bi_2MoO_6 and Bi_2WO_6 as generated by the hydrothermal method, respectively. As shown in Fig. 1a, the (131), (200), (151), (202), (133) and (280) planes of the orthorhombic Bi_2MoO_6 phase were responding to well-defined peaks at 2Ɵ= 28°, 32.4°, 36°, 46.6°, 55.2°, 56°, respectively (JCPDS card no. 21-0102) [27]. Besides, there were no additional, prominent peaks confirming Bi_2MoO_6 purity. The peaks at 2Ɵ of 27.8°, 32.8°, 47°, 55.6°, 58.4°, 68.6°, and 75.6° are assigned to (131), (200), (202), (133), (262) and (400) planes of orthorhombic Bi_2WO_6 (JCPDS, No. 39-0256), respectively as shown in Fig. 1b which are similar to patterns of Bi_2MoO_6 sample revealing the Bi_2WO_6 is also isomorphic [28]. Moreover, the diffraction peaks of Bi_2WO_6 in the range of 2θ=30-60° are higher than those of Bi_2MoO_6. Besides, no other diffraction peaks could have been caused by contaminants that indicate crystallinity [16].

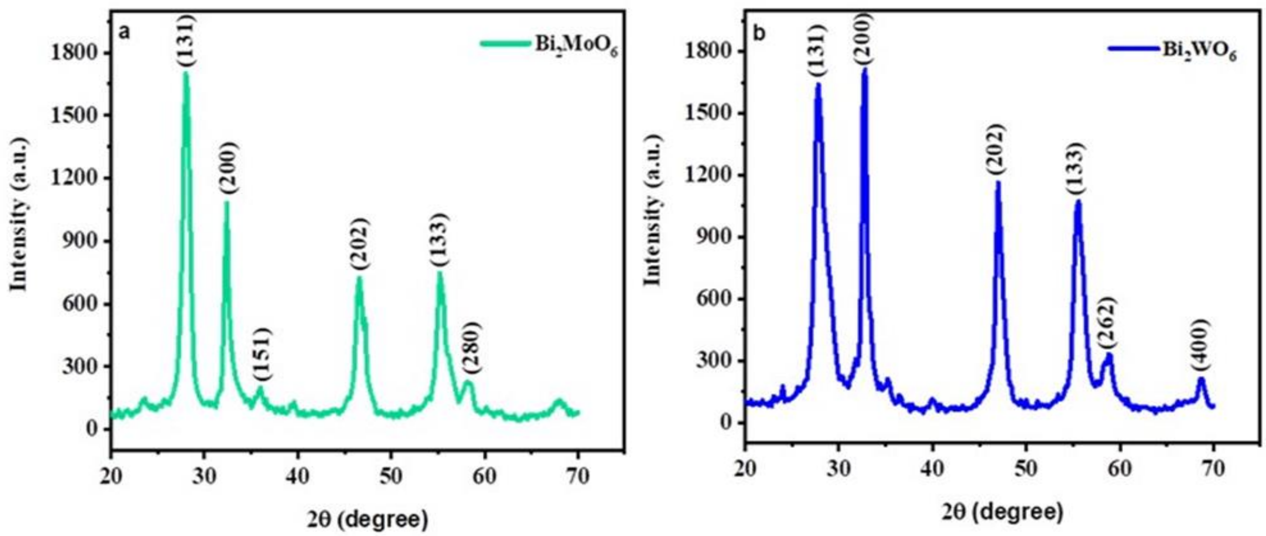

Figure 1: XRD patterns of the as-prepared a) Bi_2MoO_6 and b) Bi_2WO_6 products.

3.2 Morphological Properties

FESEM was used to characterise the microstructure and morphology of Bi_2MoO_6 and Bi_2WO_6. As shown in Fig 2a, the FESEM image of Bi_2MoO_6 nanoparticles was made up of several uneven nanosheets or typical nanoplate-like structures with smooth surfaces. Nanosheets were extremely thin, with a 40-60 nm thickness and an average width of approximately 300 nm. Furthermore, the nanosheets were tightly packed. Fig 2b shows the FESEM image of the as-prepared Bi_2WO_6. This resulted in aggregated irregular tiny flake-like Bi_2WO_6 that is made up of agglomerates of nanoplatelets with various orientations. The EDS spectrum of the Bi_2MoO_6 and Bi_2WO_6 samples were made to confirm the elemental composition and distribution homogeneity, which are shown in Fig. 2(c and d). Bi, M, and O components for Bi_2MoO_6 and Bi, W, and O components for Bi_2WO_6 are present throughout the samples. The homogenous distribution of each element in the matrix proves the samples' cleanliness.

3.3 Optical Properties

The UV-Vis spectra analysis was carried out in the 240 – 700 nm range to determine the optical properties of Bi_2MoO_6 and Bi_2WO_6, respectively. As displayed in Fig. 3 (a, b) and 4 (a, b), it was evident that the photocatalyst had a strong absorption capacity in the visible light region. As seen from Fig. 3 (a, b) and 4 (a, b), the absorption edges of Bi_2MoO_6 and Bi_2WO_6 were observed at about 300 nm and 400 nm, respectively. The absorption edge of Bi_2MoO_6 is higher than that of Bi_2WO_6. In addition, as shown in Fig. 3b and 4b, the band gaps resulted in samples Bi_2MoO_6 and Bi_2WO_6 were calculated using equation $h=A(h\upsilon-Eg)_n$ where absorption coefficient, photon energy, and general constant are all defined as α,hυ and A, respectively [29]. Using plotting αhυ against hυ (Tauc-plot), a tangent onto the linear range and extrapolation can be used to determine the band gaps.

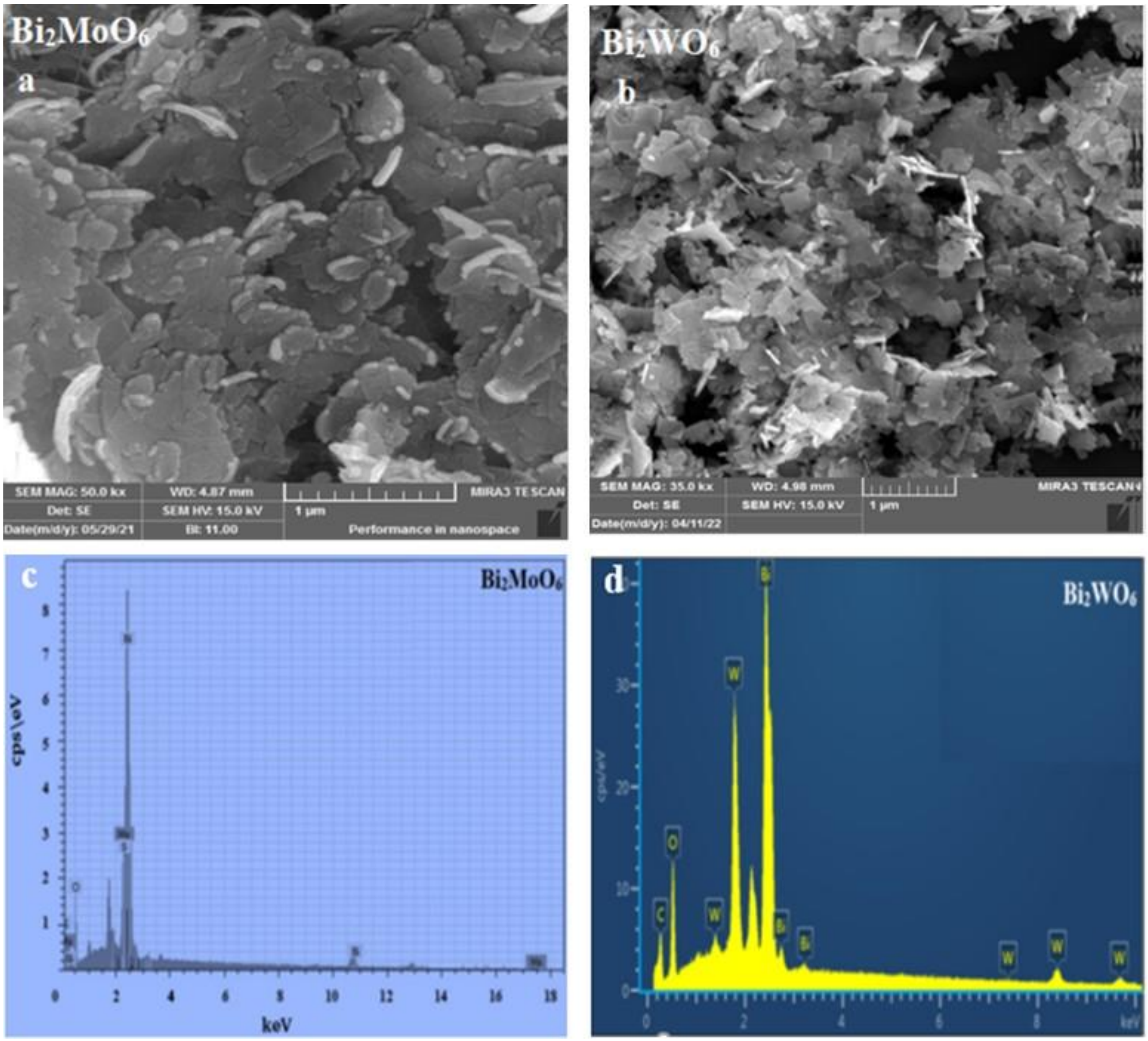

Figure 2: FESEM images (a) Bi_2MoO_6, (b) Bi_2WO_6 and EDS images (c) Bi_2MoO_6 and (d) Bi_2WO_6 samples of prepared hydrothermal technique.

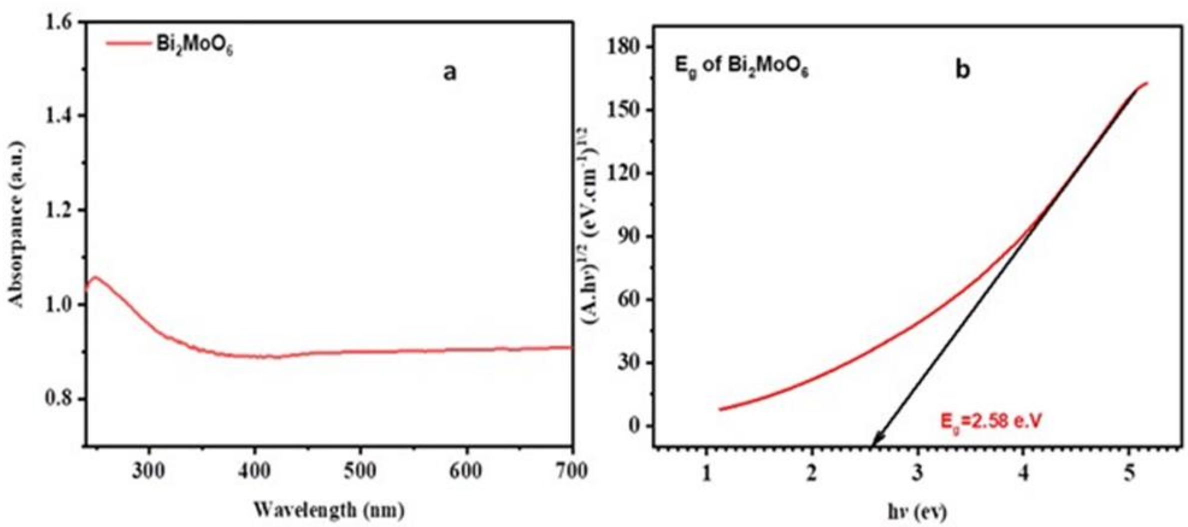

Figure 3: The UV-Vis analysis spectra of (a Bi_2MoO_6, (b energy gap Eg of Bi_2MoO_6

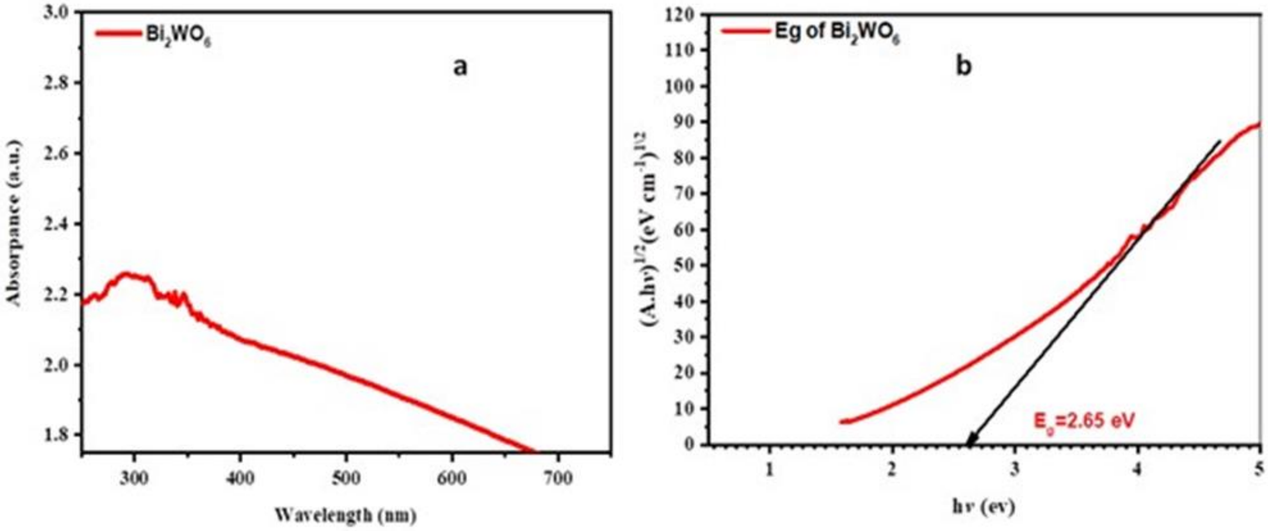

Figure 4: UV-Vis analysis spectra of (a Bi_2MoO_6, and (b energy gap Eg of Bi_2WO_6

3.4 Antibacterial Activity

To investigate the antibacterial activity of resulting Bi_2MoO_6 and Bi_2WO_6 samples against test bacteria strain *E.coli* and *S.aureus* bacteria, three different test concentrations (50, 100, and 200) µg/mL of each sample were incubated with bacterial strains at 37^{o}C for overnight without irradiation, respectively. As shown in Fig. 5a, b and 7a, b, the results indicated that the tested bacterial strain, *S.aureus*, revealed the highest zone of inhibition (24 to 29 mm) for Bi_2MoO_6 and (17.5 to 21.5 mm) for Bi_2WO_6 in the concentrations of 100 µg/mL, 200 µg\mL, respectively. In comparison, the less susceptible strain was found to be *E.coli,* which revealed a smaller zone of inhibition (15.7 to 20.3 mm) for Bi_2MoO_6 and (12.6 to 18.7 mm) for Bi_2WO_6 at concentrations of 100 µg/mL, 200 µg\mL, respectively.

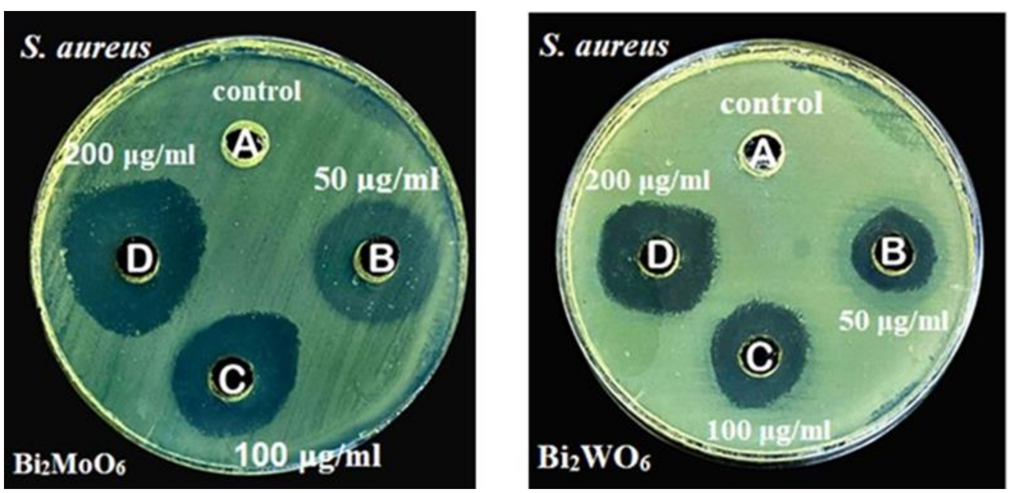

Figure 5: Images of inhibition Zone (mm) for a) Bi_2MoO_6 and b) Bi_2WO_6 against *E.coli* bacterial strain.

No inhibition zone was detected for control (DW), as shown in Fig. 6 a,b and eight a,b, respectively. Moreover, the results exhibited that the tested bacterial strain, *S.aureus* was the most susceptible bacterial strain revealing large zones of (24 mm to 29 mm) for Bi_2MoO_6 and becoming less susceptible (17.5 to 21.5 mm) for Bi_2WO_6 in the concentrations of 100 µg\mL, 200 µg\mL, respectively in comparison with the inhibition zone against tested bacterial *E.coli* as display in Fig. 7 a,b and 8 a,b.

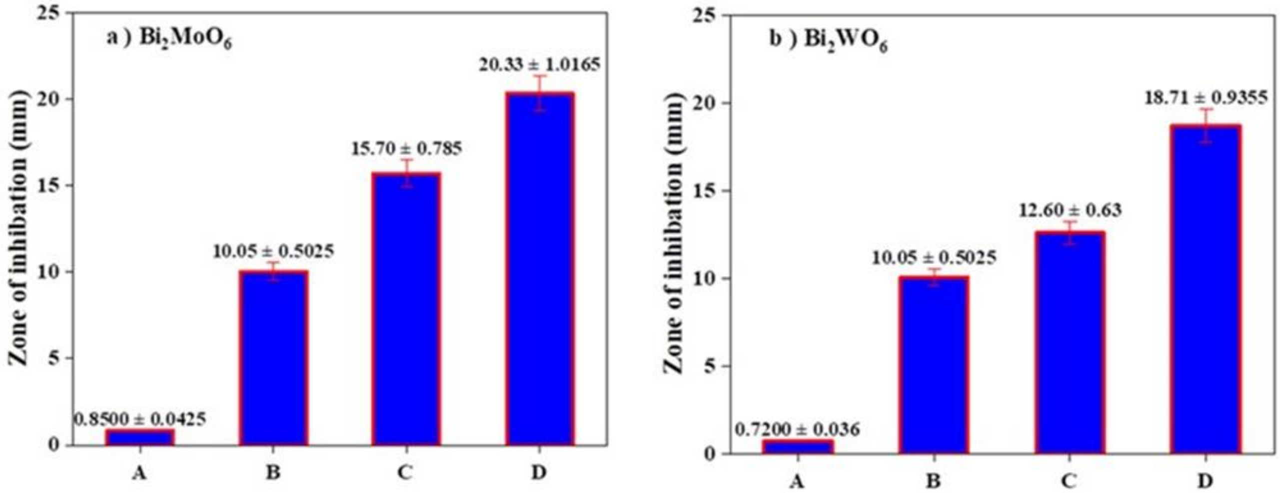

Figure 6: The Antibacterial activity of a) Bi_2MoO_6 and b) Bi_2WO_6 against *E.coli* using different content A)control, B) 50 µg/mL, C) 100 µg/mL, D) 200 µg/mL

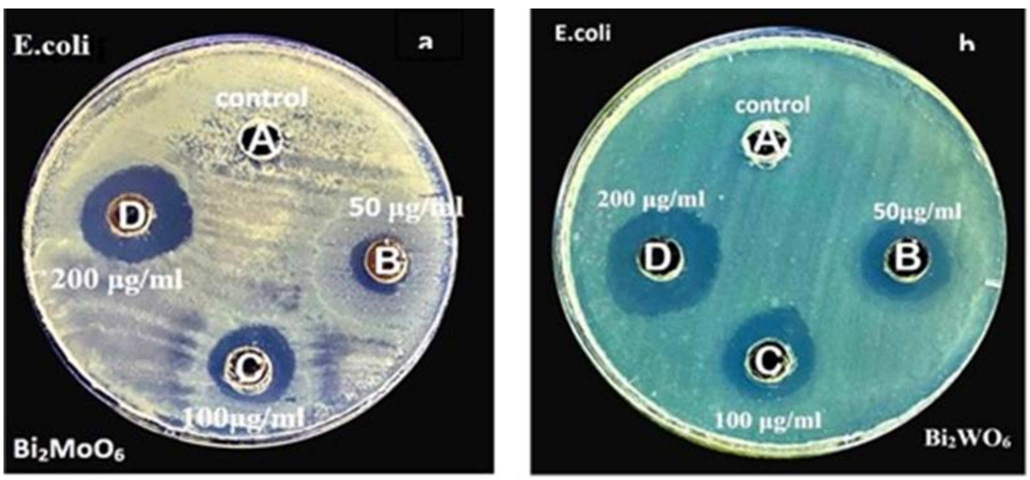

Figure7: Images of inhibition Zone (mm) for a) Bi_2MoO_6 and of b) Bi_2WO_6 against *S.aureus* bacterial strain

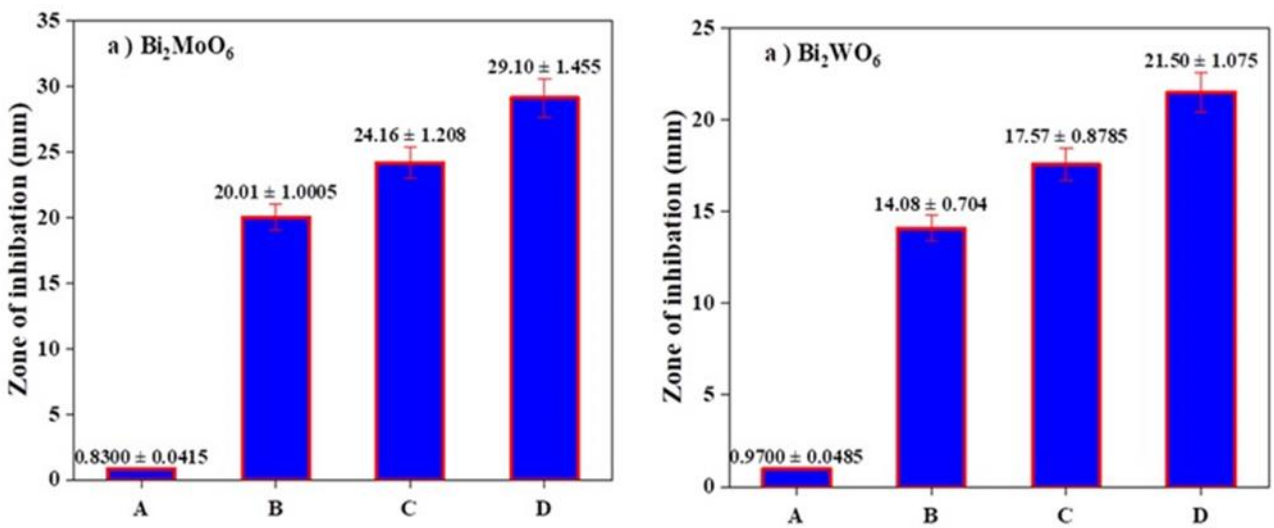

Figure 8: The Antibacterial activity of a) Bi_2MoO_6 and b) Bi_2WO_6 against S.aureus sing different contents A)control, B) 50 µg/mL, C) 100 µg/mL, D) 200 µg/mL.

These results reveal that Bi_2MoO_6 has strong antibacterial activity against *E.coli* and *S.aureus* bacteria related to possible mechanism dealing with penetration of cell membrane by Bi_2MoO_6 nanosheets as compared with Bi_2WO_6, which results in oxidation of the bacterial membrane by the effective electrostatic force between Bi-based and bacterial surface and results in the leakage of the interior component as well as improved their resistance to biological contamination [29, 30]. In addition, the interesting point to underline is that the resulting samples Bi_2MoO_6 and Bi_2WO_6 exhibited a strong effect on gram-positive and gram-negative bacteria, highlighting the great clinical and technological application [24, 31].

4. Conclusions

Bi_2MoO_6 and Bi_2WO_6 were synthesised using a hydrothermal method. The structure and morphology characterisation of fabricated samples by using FESEM, EDS, and XRD reveals the formation of a nanosheet or nanoplate-like structure with a smooth surface of each sample and the forming of orthorhombic Bi_2MoO_6 and Bi_2WO_6 phases without defects. Besides, a strong absorption capacity in the visible light region was exhibited, resulting in Bi_2MoO_6 and Bi_2WO_6. Moreover, the antibacterial activity of Bi_2MoO_6 and Bi_2WO_6 was improved against *S.aureus* bacteria. It also became less susceptible to *E. coli*, and the Bi_2MoO_6 became highly susceptible to *E. coli* and *S. aureus* bacteria related to the oxidation of the bacterial membrane by the effective electrostatic force between the Bi-based and bacterial surface.

Acknowledgement

We are grateful to Advanced Labs. in the Centre of Nanotechnology, the University of Technology, for their support of the work by making the biological tests in the Labs and providing us with the protocol for making these tests

Conflict of Interest

The authors declare that they have no conflict of interest.

References

[1] D. Lombardo, M. A. Kiselev, and M. T. Caccamo, "Smart Nanoparticles for Drug Delivery Application: Development of Versatile Nanocarrier Platforms in Biotechnology and Nanomedicine," Journal of Nanomaterials, vol. 2019, 2019.

[2] S. M. H. Al-Jawad, Z. S. Shakir, and D. S. Ahmed, "Antibacterial activity of Nickel-doped ZnO/MWCNTs hybrid prepared by sol-gel technique," European Physics Journal: Applied Physics., vol. 96, no. 2, 2021.

[3] N. Xue, L. Wang, W. Li, S. Wang, X. Pan, and D. Zhang, "Increased inheritance of structure and function of bacterial communities and pathogen propagation in plastisphere along a river with increasing antibiotics pollution gradient," Environmental Pollution., vol. 265, p. 114641, 2020.

[4] R. He, D. Xu, B. Cheng, J. Yu, and W. Ho, "Review on nanoscale Bi-based photocatalysts," Nanoscale Horizons, vol. 3, no. 5, pp. 464–504, 2018.

[5] R. He, S. Cao, P. Zhou, and J. Yu, "Recent advances in visible light Bi-based photocatalysts," Cuihua Xuebao/ Recent advances in visible light Bi-based photocatalysts, vol. 35, no. 7, pp. 989–1007, 2014.

[6] J. A. Byrne et al., "A review of heterogeneous photocatalysis for water and surface disinfection," Molecules, vol. 20, no. 4, pp. 5574–5615, 2015.

[7] L. Rizzo, A. Della Sala, A. Fiorentino, and G. Li Puma, "Disinfection of urban wastewater by solar driven and UV lamp - TiO_2 photocatalysis: Effect on a multi drug resistant Escherichia coli strain," Water Research, vol. 53, no. 0, pp. 145–152, 2014.

[8] L. Zhang, W. Wang, Z. Chen, L. Zhou, H. Xu, and W. Zhu, "Fabrication of flower-like Bi_2WO_6 superstructures as high performance visible-light driven photocatalysts," Journal of Materals Chemistry, vol. 17, no. 24, pp. 2526–2532, 2007.

[9] D. Xia et al., "Enhanced photocatalytic inactivation of Escherichia coli by a novel Z-scheme g-C_3N_4/m-Bi_2O_4 hybrid photocatalyst under visible light: The role of reactive oxygen species," Applied Catalysis B: Environmental, vol. 214, pp. 23–33, 2017.

[10] X. Wang, F. Gu, L. Li, G. Fang, and X. Wang, "A facile mixed-solvothermal route to γ-Bi_2MoO_6 nanoflakes and their visible-light-responsive photocatalytic activity," Materials Research Bulletin, vol. 48, no. 10, pp. 3761–3765, 2013.

[11] L. Zhang, T. Xu, X. Zhao, and Y. Zhu, "Controllable synthesis of Bi_2MoO_6 and effect of morphology and variation in local structure on photocatalytic activities," Applied Catalysis B: Environmental, vol. 98, no. 3–4, pp. 138–146, 2010.

[12] T. Saison et al., "New insights into Bi_2WO_6 properties as a visible-light photocatalyst," Journal Physics Chem. C, vol. 117, no. 44, pp. 22656–22666, 2013.

[13] Giannakis, S. *et al.*, "Insights into the Photocatalytic Bacterial Inactivation by Flower-Like Bi_2WO_6 under Solar or Visible Light ," Water, vol. 12, no. 1, pp. 1–19, 2020.

[14] W. Wang, G. Huang, J. C. Yu, and P. K. Wong, "Advances in photocatalytic disinfection of bacteria: Development of photocatalysts and mechanisms," Journal of Environmental Sciences (China), vol. 34, pp. 232–247, 2015.

[15] J. Tang, Z. Zou, and J. Ye, "Photocatalytic decomposition of organic contaminants by Bi_2WO_6 under visible light irradiation," Catalysis Letters, vol. 92, no. 1–2, pp. 53–56, 2004.

[16] S. Helali, M. I. Polo-Lopez, P. Fernadez-Ibanez, B. Ohtani, F. Amano, et al., "Effect of different types of supended catalyst on Escherichia coli photocatalytic inactivation under natural sunlight .," no. August, 2015.

[17] G. Tian et al., "Facile solvothermal synthesis of hierarchical flower-like Bi_2MoO_6 hollow spheres as high performance visible-light driven photocatalysts," Journal Materals Chemistry, vol. 21, no. 3, pp. 887–892, 2011.

[18] R. Shen, C. Jiang, Q. Xiang, J. Xie, and X. Li, "Surface and interface engineering of hierarchical photocatalysts," Applied Surface Science, vol. 471, no. 31, pp. 43–87, 2019.

[19] H. N. Abid, A. Al-keisy, D. S. Ahmed, A. T. Salih, and A. Khammas, "pH dependent synthesis and characterisation of bismuth molybdate nanostructure for photocatalysis degradation of organic pollutants," Environmental Science and Pollution Research, vol. 29, pp. 1–13, 2022.

[20] H. H. Bahjat, R. A. Ismail, G. M. Sulaiman & M. S. Jabir "Magnetic Field – Assisted Laser Ablation of Titanium Dioxide Nanoparticles in Water for Anti- Bacterial Applications," Journal of Inorganic and Organometallic Polymers and Materials, vol. 31, pp. 3649–3656 2021.

[21] N. Ali, A. Taha, and D. Ahmed, "Characterisation of Treated Multi-Walled Carbon Nanotubes and Antibacterial Properties," Journal of Applied Sciences and Nanotechnology, vol. 1, no. 2, pp. 1–9, 2021.

[22] H. N Abid, D. S Ahmed and A. H Al-keisy, "Constructed p-2D / n-2D BiOCl / $BiVO_4$ Nanoheterostructure for Photocatalytic Antibacterial Activity," ECS Transactions, 2022.

[23] D. S. Ahmed, N. Q. Ali, and A. A. Taha, "The Variation Effect of Mg-doped NPs Prepared by Sol-Gel Method on its Structural Properties and Biological Activities," Journal of Physics: Conference Series, vol. 2114, no. 1, 2021.

[24] Q. Feng, J. Zhou, and Y. Zhang, "Coupling Bi_2MoO_6 with persulfate for photocatalytic oxidation of tetracycline hydrochloride under visible light," Journal of Materials Science: Materials in Electronics, vol. 30, no. 21, pp. 19108–19118, 2019.

[25] C. Zhu, Y. Liu, H. Cao, J. Sun, Q. Xu, and L. Wang, "Insight into the influence of morphology of Bi WO_6 for photocatalytic degradation of VOCs under visible light," Colloids and Surfaces A: Physicochemical and Engineering Aspects, vol. 568, no. February, pp. 327–333, 2019.

[26] J. Jia et al., "Highly efficient and stable Au/Bi_2MoO_6/Bi_2WO_6 heterostructure with enhanced photocatalytic activity for NO gas removal under visible light irradiation," Journal of Physics D: Applied Physics, vol. 50, no. 14, 2017.

[27] J. Liang, F. Liu, J. Deng, M. Li, and M. Tong, "Efficient bacterial inactivation with Z-scheme AgI/Bi_2MoO_6 under visible light irradiation," Water Research, vol. 123, pp. 632–641, 2017.

[28] B. Li et al., "Superimposed surface plasma resonance effect enhanced the near-infrared photocatalytic activity of Au@Bi_2WO_6 coating for rapid bacterial killing," Journal of Hazardous Materials, vol. 380, no. July, 2019.

[29] P. Kanniah et al., "Green Synthesis of Multifaceted Silver Nanoparticles Using the Flower Extract of Aerva lanata and Evaluation of Its Biological and Environmental Applications ," ChemistrySelect, vol. 5, no. 7, pp. 2322–2331, 2020.

[30] S. Ahmed, M. Ahmad, B. L. Swami, and S. Ikram, "A review on plants extract mediated synthesis of silver nanoparticles for antimicrobial applications: A green expertise," Journal of Advanced Research, vol. 7, no. 1, pp. 17–28, 2016.

[31] Z. Khedaer, D. Ahmed, and S. Al-Jawad, "Investigation of Morphological, Optical, and Antibacterial Properties of Hybrid ZnO-MWCNT Prepared by Sol-gel," Journal of Applied Sciences and Nanotechnology, vol. 1, no. 2, pp. 66–77, 2021.